69

PROCEEDINGS

SPIE—The International Society for Optical Engineering

Wavelength Division Multiplexing Components

Louis S. Lome
Chair/Editor

29–31 January 1996
San Jose, California

Volume 2690

Polymer-based Volume Holograms for Multiple Wavelength Network Applications

Charles C. Zhou and Ray T. Chen

Microelectronics Research Center
University of Texas, Austin
Austin, TX 78758
raychen@uts.cc.utexas.edu

ABSTRACT

Wavelength division multiplexing (WDM) and demultiplexing (WDDM) devices are considered to be two of the key elements for enhancing the transmission bandwidth of optical communications and sensor systems. During the past 20 years, various type of WDMs and WDDMs have been proposed and demonstrated [1-7]. Recently the technique for producing spatially multiplexed phase grating based on polymer-based waveguide holograms for WD(D)M applications has been reported [7,8,9]. We report the formation of a surface-normal wavelength division demultiplexer using photopolymer-based volume holograms in conjugation with graded index (GRIN) lenses. The elimination of edge-coupling significantly enhances the packaging reliability and the time reversal of the beam propagation automatically results in the required wavelength division multiplexing (WDM). Furthermore, such a configuration is compatible with the implementation of vertical cavity surface-emitting lasers where the characteristic of azimuthal symmetry is maintained in the waveguiding substrate.

In this paper, we present two devices for network applications. The first is an 8 channel surface-normal WDM with a center channel wavelength of 772 nm and a wavelength separation of 4 nm. The second is a 3x3 wavelength selective crossbar with a center wavelength of 765 nm and a channel separation of 10 nm. These devices are pivotal for the realization of such a computer-to-computer interconnect network shown in Fig. 1 [1] where both wavelength division multiplexing and space division multiplexing are employed to enhance the transmission bandwidth. The switching device depicted in Fig. 1 can be realized using the wavelength-selective crossbar to be presented in this paper.

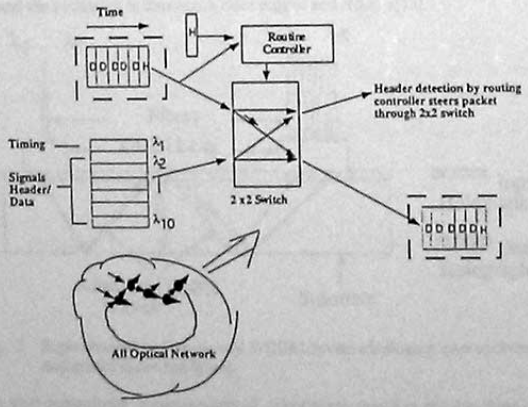

Fig. 1 JPL's Bit-Parallel Wavelength Links for High Performance Computer Networks [1]

0-8194-2064-6/96/$6.00

1. INTRODUCTION

Wavelength division multiplexing (WDM) and demultiplexing (WDDM) devices are considered to be two of the key elements for enhancing the transmission bandwidth of optical communications and sensor systems. WDDM technology enables multiple wavelengths to be packed into small optical communication windows for data transmission through one single fiber. See Fig. 2. Passive multiplexing and demultiplexing devices are used at the transmission and receiver ends to combine and separate different data channels having different wavelengths.

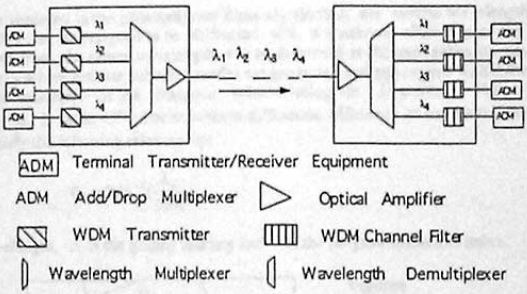

Fig. 2 Block diagram for four-wavelength wavelength-division multiplexing and demultiplexing system.

Recently, WD(D)Ms based on photo-lime gel (PLG) and photopolymer-based waveguide holograms using surface-normal coupling technique, have been reported[8,9]. In this paper, we demonstrate an 8-channel WD(D)M using collinear surface-normal input and output couplings based on the Littrow holograms packaged with GRIN rod lenses[12]. The schematic of the eight-channel WDDM device is shown in Fig. 3. The channel separation is 4 nm with center channel wavelength of 772 nm. The WD(D)M device presented herein can be integrated with transmitter and receiver modules at the surface-normal direction. As a result, pigtailing with fibers from a waveguide edge is not required and the packaging is thus much more rugged and reliable[13].

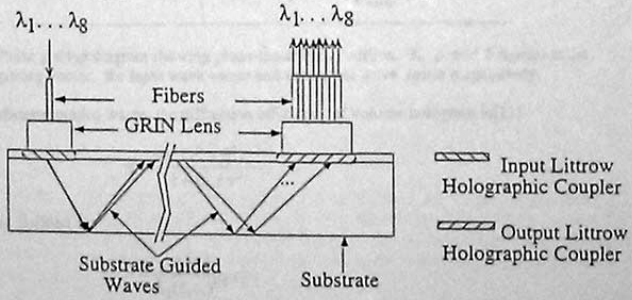

Fig. 3 Eight-channel surface-normal WDDM device employing photopolymer holographic couplers and graded index rod lenses.

We also demonstrate a surface-normal wavelength selective non-blocking crossbar based on a unique wavelength switching scheme where photopolymer-based volume holograms are employed in conjugation with graded index (GRIN) lenses. A prototype polymer-based volume hologram for multiple-wavelength 3x3 crossbar is experimentally demonstrated. The unique beam routing property of GRIN lens reduces nine wavelengths to three wavelengths while maintaining the required nine (3 x 3) individual interconnects. The elimination of edge-coupling significantly enhances the packaging reliability. Furthermore, such a configuration is compatible with the

implementation of vertical cavity surface-emitting lasers. In the present devices, the characteristic of azimuthal symmetry is maintained in the waveguide substrate due to the employment of substrate guided waves[12].

2. EIGHT-CHANNEL WDDM DEVICE

2.1. POLYMER-BASED VOLUME PHASE HOLOGRAM COUPLER

The phase gratings recorded in the photopolymer films are slanted, the central wavelength of the input surface-normal beam, i.e., 772 nm, is designed to be diffracted with a maximum efficiency at the Bragg angle. The wavelengths that deviate from the center wavelength will be dispersed at different substrate bouncing angles with less diffraction efficiency where discrete substrate modes are generated and zig-zagged within the substrate[3]. The schematic of the micro structure of the designed volume hologram is shown in Fig. 4. The central wavelength bouncing angle θ_0 is set at 45°. For maximum diffraction efficiency at the central wavelength, the grating spacing Λ must satisfy the following relationship:

$$\theta_0 = 2\sin^{-1}\left(\frac{\lambda_0}{2n\Lambda}\right), \tag{1}$$

where λ_0 is the central wavelength, Λ is the grating spacing and n is the polymer refractive index.

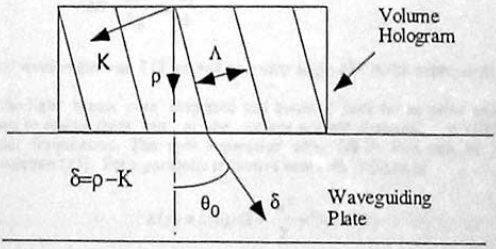

Fig. 4 Phase grating diagram showing phase-matching condition. K, ρ and δ represent the grating vector, the input wave vector and the output wave vector respectively.

For TE substrate-guided waves, the diffraction efficiency of volume hologram is[11]

$$\eta = \frac{\sin^2(v^2+\xi^2)^{1/2}}{1+\xi^2/v^2}, \tag{2}$$

with the parameters defined as

$$v = \frac{\pi\Delta n d}{\lambda_0(c_r c_s)^{1/2}}, \tag{3}$$

$$\xi = -\frac{\Delta\lambda K^2 d}{8\pi n c_s} = \frac{\Delta\theta K_d \sin\Phi}{2c_s}, \tag{4}$$

$$c_r = 1, \quad c_s = 1 - \frac{K\cos\Phi}{k_0}, \tag{5}$$

$$K = \frac{2\pi}{\Lambda}, \qquad k_0 = \frac{2\pi}{\lambda_0}, \tag{6}$$

$$\Phi = \frac{180^\circ - \theta_0}{2}, \tag{7}$$

where Δn is the refractive index modulation, $\Delta\lambda$ is wavelength difference of channel λ_i from center wavelength λ_0.

2.2. CHROMATIC DISPERSION AND CHANNEL SEPARATION

From Eqn. (4) we can see that the change of wavelength from central wavelength corresponds to the change of diffraction angle. The angular differences among different wavelengths were maintained as they were bounced in the substrate. An angular frequency filter, such as an aspherical lens or a GRIN rod lens, can be used to separate light channels with different angles. A quarter pitch GRIN lens was employed to separate light beams with different wavelengths and they focused onto the output surface of a GRIN lens which functions as an output coupler connecting to a fiber array (Fig. 4).

The angular separation due to dispersion can be derived from the Bragg condition $\cos\Phi = \frac{K}{2nk_0}$ and Eqn. (1) as

$$\Delta\theta = \frac{\Delta\lambda}{\lambda_0}\tan\frac{\theta_0}{2}, \tag{8}$$

where the central wavelength was 772 nm and bouncing angle 45° in the experiment.

After the light beams were dispersed and bounced back to the same side of the substrate, a hologram coupler was used to couple them out at the surface normal direction. A GRIN lens is used to separate the different angular frequencies. The spot separation after GRIN lens can be predicted using paraxial ray approximation solution [15]. For a parabolic refractive index distribution of

$$n(y) = n(0)\cdot\left(1 - \frac{A^2}{2}y^2\right), \tag{9}$$

the ray path can be predicted using

$$\begin{bmatrix} y_3 \\ \alpha_3 \end{bmatrix} = \begin{bmatrix} \cos(Az) & \frac{n_0}{n_1 A}\sin(Az) \\ -\frac{n_2}{n_3}A\sin(Az) & \frac{n_0 n_2}{n_1 n_3}\cos(Az) \end{bmatrix} \cdot \begin{bmatrix} y_0 \\ \alpha_0 \end{bmatrix}, \tag{10}$$

where y is the radial distance from GRIN lens axis, z is axial distance from GRIN lens input surface, A is the GRIN lens constant, n_0 and n_3 are the refractive indexes of the input and the output media of GRIN lens, n_1 and n_2 are the refractive indexes of the GRIN lens at the input and the output positions of the optical beam, y_0 and α_0 are respectively the input position and the angle of the beam at the input, and y_3 and α_3 are the output position and the angle of the beam in the output medium (Fig. 5).

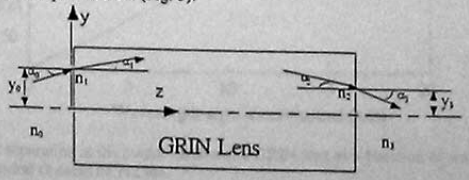

Fig. 5 Schematic of ray tracing about GRIN lens.

For $Az = \pi/2$, i.e., a quarter pitch GRIN pitch lens, the cosine term diminishes; therefore, the incoming beams with a same wavelength and $\alpha_0(\Delta\theta)$ will eventually come out from the same spot of the GRIN lens output surface regardless of the input positions. From Eqn. (10) we can see that the focusing effect is symmetric to the output surface-normal regardless of the location of input spot. Such a property facilitates coupling with fibers. The paths of rays with the same incident angle but different positions are illustrated in Fig. 6 for a quarter pitch GRIN lens. The channel separation from the GRIN lens output surface can be calculated from Eqn. (10) where GRIN lens was a quarter pitch, and the GRIN lens constant A was 0.046 mm^{-1} in our experiment. The central wavelength for the 8-channel WDM was 772 nm, 4 nm channel separation was set for neighboring channels. On the input GRIN lens surface, the central wavelength was incident surface-normally while channel angular separation of $\Delta\theta = 0.2^o$ was set for each neighboring channel. At the output surface of the GRIN lens, rays with the same bouncing angle of incidence converged at the same spot as we predicted. The wavelength-dependent incident angles were provided by the dispersive volume hologram. The use of GRIN lens provides the capability of surface mounting for holograms and fibers and thus it's more reliable and compact.

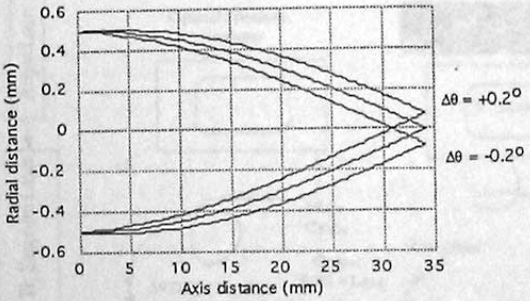

Fig. 6 Ray tracing of light with different incident angle onto the quarter pitch output GRIN lens.

Based on the hologram coupler properties and GRIN lenses parameters discussed above, we calculated the output spot separation as a function of wavelength migration using Eqn. (4) and Eqns. (9) and (10). The theoretical result is plotted in Fig. 7. The channel separation after the output GRIN lens surface dictates the determination of the wavelength separation and corresponding crosstalk level.

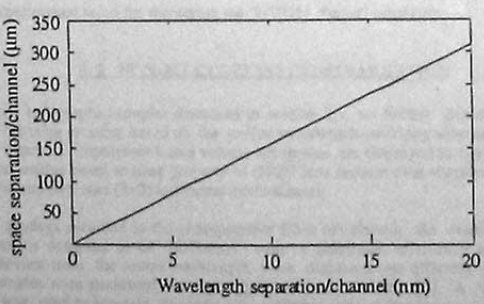

Fig. 7 Output spot separation at the output surface of a GRIN lens as a function of wavelength deviating from the central channel of 772 nm.

3. EXPERIMENTAL RESULTS

3.1. EIGHT-CHANNEL WDDM

The experimental setup for eight WDDM is shown in Fig. 8. A Ti:sapphire tunable laser was pumped by an Innova 200 Argon laser. A microscopic objective focused the TE light waves into a single mode fiber which had a quarter pitch GRIN rod collimator attached on the other end. The input light was monitored by an optical spectrum analyzer. The collimated light from the single mode fiber was diffracted by the input hologram coupler and then zig-zagged inside the waveguiding plate. It was subsequently coupled out by the output hologram. The output GRIN rod lens focused the light beams with different incident angles to different spots corresponding to different wavelengths. A CCD camera took the pictures. Such parameters as spot size, channel separation and crosstalk were measured. In our experiment using components as described in the simulation, the average channel separation was 80 μm and average spot size less than 60 μm. The average crosstalk was less than -20 dB.

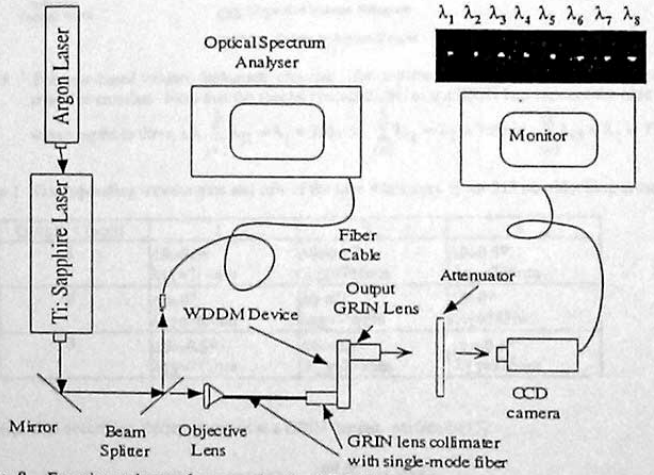

Fig. 8 Experimental setup for measuring the WDDM channel separation.

3.2. NON-BLOCKING 3X3 CROSSBAR SWITCH

Based on the holographic coupler discussed in section 2.1, we further demonstrate the formation of a surface-normal non-blocking crossbar based on the unique wavelength switching scheme. The demonstrated device is shown in Fig. 9 where photopolymer-based volume holograms are employed in conjugation with graded index (GRIN) lenses. The unique beam routing property of GRIN lens reduces nine wavelengths to three wavelengths while maintaining the required nine (3x3) individual interconnects.

The phase gratings recorded in the photopolymer films are slanted, the central wavelength of the input surface-normal beam is designed to be diffracted with a maximum efficiency at the Bragg angle. The wavelengths that deviate from the center wavelength were dispersed into different substrate bouncing angles. Discrete substrate modes were generated and zig-zagged within the substrate[3]. A GRIN lens after the output hologram coupler was used to separate channels with different angular frequencies. For a GRIN lens having a parabolic refractive index distribution profile (Eqn. (9)), the paraxial ray tracing can be predicted using Eqn. (10). The wavelengths and the variations of $\Delta\theta$ are summarized in Table 1. The results of the simulation is shown in Fig. 10 where the GRIN lens is a quarter pitch having a GRIN lens constant A of 0.046 mm^{-1}.

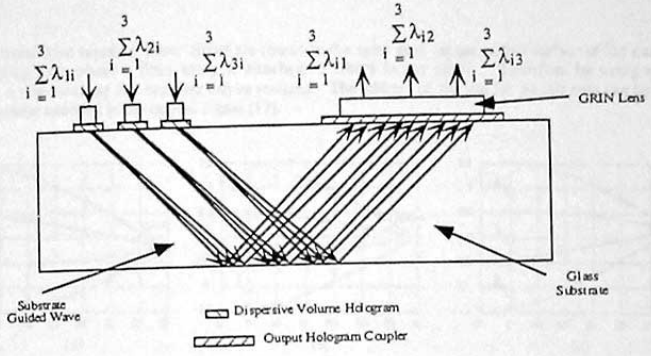

Fig. 9 Polymer-based volume hologram crossbar for a surface-normal 3x3 non-blocking wavelength selective crossbar. Note that the special characteristic of the GRIN lens reduces the nine wavelengths to three, i.e. $\sum_{i=1}^{3}\lambda_{i1}=\lambda_1=755\text{nm}$, $\sum_{i=1}^{3}\lambda_{i2}=\lambda_2=765\text{nm}$, $\sum_{i=1}^{3}\lambda_{i3}=\lambda_3=775\text{nm}$.

Table 1 Corresponding wavelengths and $\Delta\theta$s of the nine interconnects for 3x3 non-blocking crossbar.

Output \ Input	1	2	3
1	$\Delta\theta=0.5^o$ $\lambda_{11}=755\text{nm}$	$\Delta\theta=0.5^o$ $\lambda_{21}=755\text{nm}$	$\Delta\theta=0.5^o$ $\lambda_{31}=755\text{nm}$
2	$\Delta\theta=0^o$ $\lambda_{12}=765\text{nm}$	$\Delta\theta=0^o$ $\lambda_{22}=765\text{nm}$	$\Delta\theta=0^o$ $\lambda_{32}=765\text{nm}$
3	$\Delta\theta=-0.5^o$ $\lambda_{13}=775\text{nm}$	$\Delta\theta=-0.5^o$ $\lambda_{23}=775\text{nm}$	$\Delta\theta=-0.5^o$ $\lambda_{33}=775\text{nm}$

The paraxial equation describing the ray position at a GRIN output surface is[15]:

$$y(L)=y_0\cos(AL)+\frac{\tan(\Delta\theta)}{A}\cdot\sin(AL), \tag{11}$$

where p is the pitch size of the GRIN lens, the $L=2\pi p/A$ is the length of the GRIN lens. Note for a quarter pitch lens, i.e., p=1/4, only the second term of Eqn. (11) exists; therefore, incoming beams with the same wavelength and $\Delta\theta$ came out from the same spot at the output surface of the GRIN lens. In our experiment, the corresponding λ_{ij} and $\Delta\theta$ for each case of the 3x3 crossbar interconnects are summarized in Table. 1. An array of three GRIN lens with 1 mm diameter each was used to collimating light to the input hologram coupler. λ_{1i} and λ_{3i} (i=1, 2, 3) were incident 1 mm off the center of the output GRIN lens axis (Fig. 9). On the output surface, rays with the same initial angle of incidence converge at the same spot as we predicted. Therefore, employment of GRIN lens reduces nine wavelengths to three wavelengths while keeping the required interconnectivity. The incident angle differences are provided by the dispersive volume hologram. The use of GRIN lens provides the capability of surface mounting for holograms and fibers. A reliable miniaturized packaging can be provided.

In the configuration shown in Fig. 9, three input fibers each with a collimating GRIN lens at its end are attached surface normally to the input holographic coupler. The three wavelengths transmitted through one single fiber are dispersed by volume hologram into three different bouncing angles. As described by Eqn. (10), a quarter pitch output GRIN lens separates light with different colors (i.e. wavelength). The signal beams with a same

wavelength from three separate input fibers are routed to the same spot at the output surface of the quarter pitch GRIN lens (Fig. 10), where a fiber array is attached (3 fibers in our case). Therefore by using only three wavelengths, a non-blocking 3x3 crossbar can be realized. The address of the sender in this case can be identified through the header encoded in the optical signal [17].

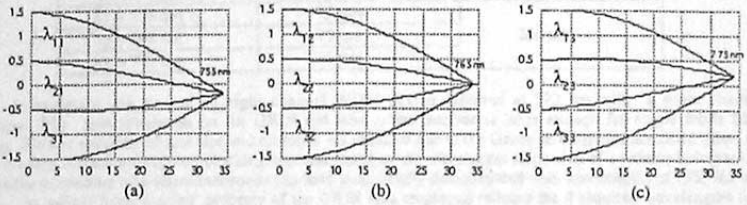

Fig. 10 Ray tracing of light with different incident angles from three input angular dispersed light beams onto the quarter pitch output GRIN lens (a) $\sum_{i=1}^{3} \lambda_{i1} = \lambda_1 = 755\text{nm}$ (b) $\sum_{i=1}^{3} \lambda_{i2} = \lambda_2 = 765\text{nm}$, (c) $\sum_{i=1}^{3} \lambda_{i3} = \lambda_3 = 775\text{nm}$.

The experimental setup for 3x3 crossbar testing is similar to that of Fig. 8. A different device was made for this demonstration. A Ti:sapphire tunable laser was pumped by a continuous Argon Ion laser. DuPont polymer film HRF-600 having a thickness of 20 μm was employed and the hologram was recorded at 514 nm. The volume hologram was fabricated using two beam interference method[14]. A microscopic objective coupled the light into a single mode fiber which had a GRIN rod lens attached at the output end. The input wavelength was monitored by an optical spectrum analyzer. The collimated light from the single mode fiber was diffracted by the input holographic coupler and zig-zagged inside the glass substrate, and was subsequently coupled out by the output hologram coupler. The output GRIN rod lens focused the light onto different spots corresponding to different wavelength channels. A CCD camera and an eight bit frame grabber image processing system was employed to take the pictures. Spot size, channel separation and other parameters were experimentally confirmed(Fig. 11). In our experiment, the average channel separation was 250 μm and average spot size less than 60 μm. The average

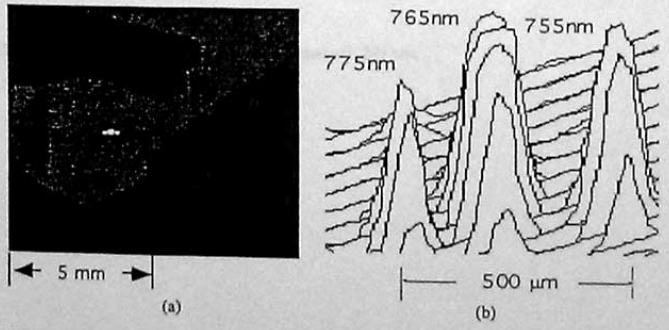

Fig. 11 (a) Image of GRIN lens output surface showing three-wavelength channel separation (b) Three-dimensional intensity profile of the three spots shown in (a).

crosstalk was less than 20 dB. A summary of results is given in Table 2. The output spectrum of 775 nm channel is shown in Fig. 12. It's found that the output spectrum has the same bandwidth as that of the input (not shown). It's also true for other channels. Due to the Gaussian beam nature of the substrate guided waves, the output spots are larger than the diffraction limited spots. Such an effect will be evaluated in a separate publication.

Table 2 The measurement result of three-wavelength non-blocking crossbar.

Wavelength	Spot Size (3 dB)	Channel Separation
λ_1 = 755 nm	75 μm	250 μm
λ_2 = 765 nm	75 μm	
λ_3 = 775 nm	75 μm	

In summary, we present an eight channel WDM device centered at 772 nm with a 4 nm channel separation. The spot separation on the GRIN rod lens output surface is large enough for single mode fiber coupling. Further reducing of spot size and crosstalk are required due to the Gaussian beam characteristic. Also, we present the first surface-normal non-blocking crossbar based on the wavelength dispersion of a volume hologram. A 3x3 crossbar containing nine interconnections has been successfully demonstrated with wavelengths of 755, 765 and 775 nm. The unique beam routing property of the GRIN lens employed reduces the 9 required wavelengths to 3 while maintaining the 3x3interconnections.

This research is sponsored by AFOSR, BMDO and ARPA's Center for Optoelectronics Science and Technology. The authors thank Maggie M. Li for her help.

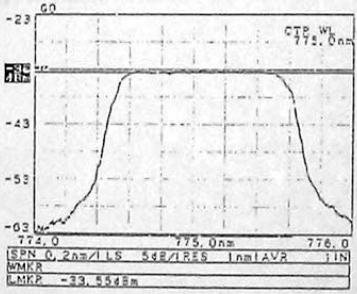

Fig. 12 Output spectrum of the 3x3 crossbar at channel 775 nm.

REFERENCES

1. L. A. Bergman, A. J. Mendez and L. S. Lome, SPIE Critical Review, 1996
2. W.J. Tomlinson, Appl. Opt. 16(8), 2180 (1977).
3. A.C. Livanos, A. Katzir, A. Yariv, and S.C. Hong, Appl. Phys. Lett. 30(10), 519(1977).
4. H. Ishio, J. Minowa, and K. Nosu, J. of Lightwave Tech. 2(4), 448 (1984).
5. H. Obara and Y. Hamazumi, Electron. Lett. 28(13), 1268 (1992).
6. A.E. Willner, C.J. Chang-Hasnain, and J. E.Leight, IEEE Photonics Tech. Lett. 5(7), 838 (1993).
7. Y.T. Huang, D.C. Su, and Y.K. Tsai, Opt. Lett. 17(22), 1629(1992).
8. M. R. Wang, G. J. Sonek, R. T. Chen, and T. Jannson, IEEE Photonics Tech. Lett. 3(1), 36 (1991).
9. M. M. Li, R. T. Chen, Sunning Tang, and Dave Gerold, Appl. Phys. Lett. 65(9), 1070(1994).
10 Y. T. Huang, D. C. Su, and Y. K. Tsai, Opt. Lett. 17(22), 1629(1992).
11. H. Kogelnik, The Bell Sys. Tech. J. 48(9), 2909 (1969).
12. M. M. Li, and R. T. Chen, Opt. Lett. 20(7), 797(1995).
13. R.T.Chen, H. Lu, D.Robinson, and T.Jannson, App. Phys. Lett. 59(10), 1144 (1991).
14 R. T. Chen, S. Tang, M. M. LI, D. Gerold, and S. Natarajan, Appl. Phys. Lett. 63, 1883(1993).
15. W. M. Rosenblum, J. W. Blaker and M. G. Block, American Journal of Optometry and Physiological Optics, 65(8), 661(1988).
16. A. Yariv, Optical Electronics, 4th edition pp.47 (Winston Inc., 1991).
17. IEEE Standard for Scalable Coherent Interface (SCI), IEEE STD 1596-1992.